

Provided for non-commercial research and education use.
Not for reproduction, distribution or commercial use.



This article appeared in a journal published by Elsevier. The attached copy is furnished to the author for internal non-commercial research and education use, including for instruction at the authors institution and sharing with colleagues.

Other uses, including reproduction and distribution, or selling or licensing copies, or posting to personal, institutional or third party websites are prohibited.

In most cases authors are permitted to post their version of the article (e.g. in Word or Tex form) to their personal website or institutional repository. Authors requiring further information regarding Elsevier's archiving and manuscript policies are encouraged to visit:

<http://www.elsevier.com/authorsrights>



A method for reducing the energy consumption of pick-and-place industrial robots

M. Pellicciari, G. Berselli*, F. Leali, A. Vergnano

Department of Mechanical and Civil Engineering, University of Modena and Reggio Emilia, Via Vignolese 905, 41125 Modena, Italy

ARTICLE INFO

Article history:

Received 19 April 2012

Accepted 27 January 2013

Available online 13 March 2013

Keywords:

Energy efficiency

Virtual prototyping

Robotic manufacturing

Electromechanical modeling

ABSTRACT

The interest in novel methods and tools for optimizing the energy consumption in robotic systems is currently increasing. From an industrial point of view, it is desirable to develop energy saving strategies also applicable to established manufacturing systems with no need for either hardware substitution or further investments. Within this scenario, the present paper reports a method for reducing the total energy consumption of pick-and-place manipulators for given TCP position profiles. Firstly, electromechanical models of both serial and parallel manipulators are derived. Then, the energy-optimal trajectories are calculated, by means of constant time scaling, starting from pre-scheduled trajectories compatible with the actuation limits. In this manner, the robot work cycle can be energetically optimized also when the TCP position profiles have been already defined on the basis of technological constraints and/or design choices aimed at guaranteeing manufacturing process efficacy/robustness. The effectiveness of the proposed procedure is finally evaluated on two simulation case studies.

© 2013 Elsevier Ltd. All rights reserved.

1. Introduction

The development of energy efficient mechatronic systems is currently changing standard paradigms in the design and control of robotic devices. Many approaches for Energy Consumption (EC) minimization are found in different research fields, such as introduction of energy efficient equipments or renewable energy sources, optimal hardware selection and path planning, up to the optimization of the overall production plant [1]. Nonetheless, it is self-evident that these strategies involve substantial investments and are applicable on different time frames. In fact, renewable energies will find a global impact in a mid/long term goal [2] whereas novel equipments (e.g. lightweight robots [3]) might not be readily applied to real systems due to market constraints, such as costs and/or production rates. Still, most energy saving methods described in literature rely on either plant modification or path re-planning and, therefore, are realistically adopted only in the initial plant design process.

For instance, energy optimization for electromechanical hardware is well investigated in e.g. [4]. In [5], a selection of off-the-shelf robots is made regarding their EC for a specified operation. Many past researches concern energy-optimal paths and motion profiles, considering the system dynamics and control, see e.g. [6–10]. In the field of autonomous robots (see e.g. [11,12]), EC can be regarded as a possible cost function to be minimized in

order to determine optimal design parameters (such as gear reduction ratios, actuator placements, etc. [13,14]).

On the other hand, for what concerns industrial applications, an effective method for optimizing an established system must trade off between the involved fixed costs for new equipments and the reduction of the variable costs for energy. Also, these systems are usually technologically optimized and liable of small possibilities for adjustments due to quality issues. Therefore, when a production line is in this mature lifecycle phase, it is surely desirable to reduce the EC while involving little changes and no further investments. In particular, a large possibility of improvement concerns existing robotic manufacturing cells which are far from their lifecycle end and are kept productive without substantial modifications.

Within this scenario, the focus of this paper is to present a novel and effective method for minimizing the EC of industrial robots characterized by either serial or parallel kinematic structure. The method can be employed for designing optimal pick-and-place operations which are firstly defined on the basis of manufacturing effectiveness and/or technological constraints (e.g. strictly sequential assembly operations) and are then optimized in terms of overall EC. Differently from previously published solutions, the electromechanical parameters (i.e. hardware characteristics) and the joint position profiles (and, consequently, the end-effector path) are assumed as given, the only design variable being the Task Execution Time (TET), T_O . In fact, a strong modification of the TCP motion law might be practically unfeasible, due to the intrinsic limitation of industrial controllers and due to the aforementioned process constraints. Nonetheless, in many industrial applications (e.g. manipulation or spot welding operations), the TET can be

* Corresponding author. Tel.: +39 3358092364.

E-mail addresses: marcello.pellicciari@unimore.it (M. Pellicciari), giovanni.ber-selli@unimore.it (G. Berselli), francesco.leali@unimore.it (F. Leali), alberto.vergnano@unimore.it (A. Vergnano).

assessed in order to obtain a process scheduling characterized by both energy-optimality and compatibility with the cell production rates [15].

The concept is well described considering a pick-and-place operation performed by a 6 degrees of freedom (d.o.f.) anthropomorphic arm or by a common 3 d.o.f. Parallel Kinematic Machine. As qualitatively depicted in Fig. 1a, let consider a time frame $t \in [0, T_F]$, T_F being the cycle time, and let suppose the robot end effector is executing cyclic pick-and-place operations for $t \in [0, T_O]$ whereas it is kept stationary, in a configuration $\mathbf{q}_d(T_O)$, for $t \in [T_O, T_F]$ (idle time). Suppose the handled object is carried for $t \in [T_A, T_B] \subset [0, T_O]$, whereas the robot homing motion is performed for $t \in [T_B, T_O]$ (homing time).

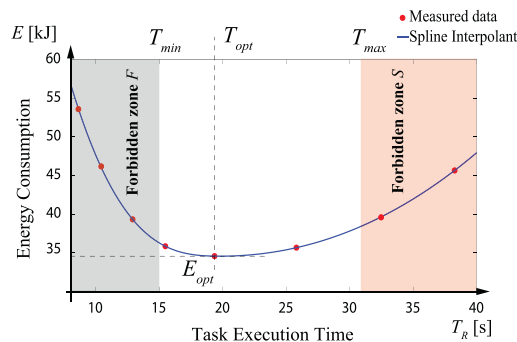
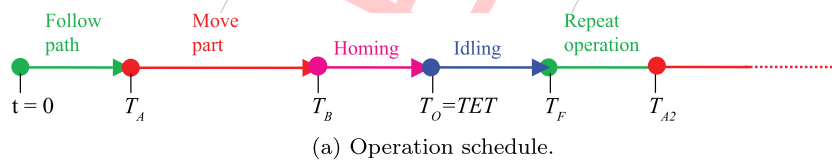
The overall EC during the operation is depicted in Fig. 1b as a function of TET. The energy needed to perform the operation increases, with respect to a global optimum T_{opt} , for both low and high TET (i.e. fast or slow speed respectively). On the other hand, most scheduling optimization methods (e.g. time-optimal point to point motions [16]), assume that the robot operates at its maximum speed, whenever allowed by the scheduling constraints, and stands still otherwise. However, such task planning strategy may be energetically detrimental, leading to high power consuming accelerations and longer idle times (where energy is wasted to counteract gravitational loads). This condition of maximum speed is also commonly adopted concerning the robot's homing motion, whose duration might be altered without any violation of the process constraints, here including the production rates. According to very recent researches [17], the idle and homing times for industrial robots in the automotive industry amount respectively to 74% and 15–20% of the total working times. Hence, the possibility to improve the system efficiency without varying the cycle time, T_F , really seems substantial. Note that, in any case, very low TET cannot be achieved due to limitations in the nominal torque of the actuation system (forbidden zone F in Fig. 1b), whereas very high TET are considered forbidden as long as they might negatively affect the production rate (forbidden zone S in Fig. 1b).

The conceptual steps of the method described in the following sections are depicted in Fig. 2. Starting from pre-scheduled joint trajectories compatible with the process constraints, the actuator torques are computed. The overall power consumption is then calculated by introducing the actuators lumped-parameters model. At last, the energy consumption as function of TET is determined by means of time scaling [18].

To the best of the authors' knowledge, the contribution of the present paper with respect to previous literature and, in particular, with respect to [15] where the method was firstly introduced, include: (a) the presentation of preliminary experimental results (Section 2); (b) the extension of the method to PKM dynamics (Section 6); (c) the definition of an efficiency measure which allows to evaluate, under certain simplifying conditions, the efficacy of the method without previous knowledge of the actuator parameters (Section 6.1). Also, differently from some previous literature (see e.g. [19,15,20]), a clear interpretation of the energy flow through the system in terms of energy stored, transferred to the user, or dissipated is highlighted, such that dissipative terms are minimized whereas conservative terms (which do not contribute to the energy consumption) and terms which cannot be optimized (i.e. useful work) are simply neglected. After the presentation of preliminary experiments, two simulation case studies are finally discussed concerning a serial and a parallel robot. Numerical results show the possibility to reduce the system EC with virtually no effects on the overall productivity.

2. Preliminary experimental results

At first, a proof-of-concept experimental campaign has been carried out prior to the development of the mathematical model. The experimental set up, schematized in Fig. 3, is similar to the one described in [21] and features an ABB IRB6600-225/2.25 antropomorphic arm connected to a wattmeter IRS MeetBOX-25P with analog input module NI 9205. The wattmeter probes are plugged into the controller cabinet and monitor the three phases 380 VAC voltages and currents supplied to the robot (including the controller itself and excluding all other resources within the workcell). For fixed measurement times T_F (Fig. 1a), the robot is programmed to follow a circular path in a vertical plane, at increasing velocities and idle times, while voltages and currents are monitored with 10 kHz sampling frequency. The overall EC is then computed by postprocessing the data in Matlab, as in [21], and successively fitted with a spline interpolant, as shown in Fig. 1b. The reported experimental values highlight the existence of an EC minimum for the considered operation. Naturally, concerning manufacturing lines where a large number of robots is performing different tasks (each being characterized by its own energy curve), it is certainly not convenient, in terms of time and costs, to determine the EC



(b) Energy Consumption as a function of TET, T_O .

Fig. 1. Energy consumption in pick-and-place operations.

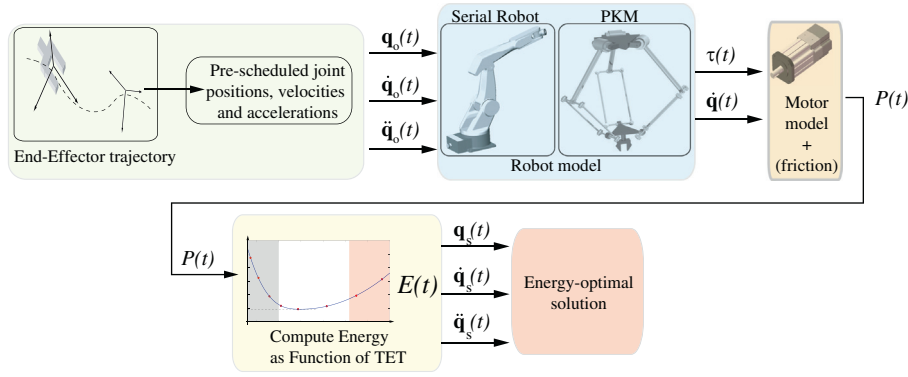


Fig. 2. Calculation of the energy consumption.

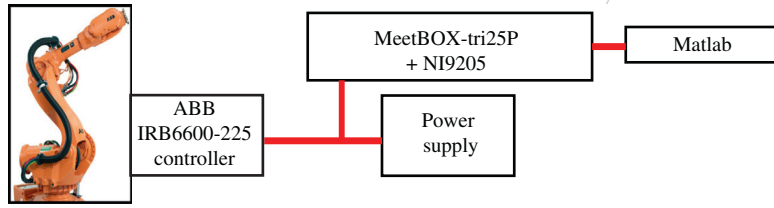


Fig. 3. Experimental set-up schematic.

minimum by means of experiments. Hence, as shown in the following, the development of a numerical method which enables the prediction of the energy-optimal TET for a generic operation is fully motivated.

3. Electro-mechanical modeling of industrial robots

3.1. Background on serial manipulators dynamic model

A typical n -link serial manipulator (an open kinematic chain), as shown in Fig. 2, is actuated by n Permanent Magnet (PM) synchronous machines. In case of pick-and-place operations, the vector of actuation torques, $\tau_r \in \mathbb{R}^n$, can be expressed as the sum of the following terms:

$$\tau_r = \underbrace{\mathbf{M}_r(\mathbf{q}_r)}_{\tau_{ri}} \ddot{\mathbf{q}}_r + \underbrace{(\mathbf{I}_n \otimes \dot{\mathbf{q}}_r^T)}_{\tau_{rc}} \begin{bmatrix} \mathbf{V}_{1r}(\mathbf{q}_r) \\ \vdots \\ \mathbf{V}_{nr}(\mathbf{q}_r) \end{bmatrix} \dot{\mathbf{q}}_r + \underbrace{\frac{\partial H_r(\mathbf{q}_r)}{\partial \mathbf{q}_r}}_{\tau_{rg}} + \mathbf{J}_r^T(\mathbf{q}_r) \left[\underbrace{m\ddot{\mathbf{r}}}_{\mathbf{h}_f} + \underbrace{[\mathfrak{I}\dot{\omega} + \omega \times \mathfrak{I}\omega]}_{\mathbf{h}_c} + \underbrace{[mg]}_{\mathbf{h}_g} \right] \quad (1)$$

where $\mathbf{q}_r \in \mathbb{R}^n$ is the vector of joint positions, $\mathbf{M}_r(\mathbf{q}_r) \in \mathbb{R}^{n \times n}$ is the symmetric joint-space inertia matrix, $\mathbf{V}_{ir}(\mathbf{q}_r) \in \mathbb{R}^{n \times n}$ ($i = 1, n$) describes the Coriolis/centripetal torques ($\mathbf{I}_n \in \mathbb{R}^{n \times n}$ denoting the identity matrix and \otimes denoting the Kronecker product, see [22], pp. 127, [23], pp. 128.), $H_r(\mathbf{q}_r)$ is the arm potential energy, $\mathbf{J}_r(\mathbf{q}_r) \in \mathbb{R}^{n \times n}$ is the manipulator Jacobian matrix, m is the mass of the handled object, $\mathbf{g} \in \mathbb{R}^3$ is the gravity vector (in appropriate units and direction), $\mathfrak{I} \in \mathbb{R}^{3 \times 3}$ is the inertial matrix of the object, and $\mathbf{0} \in \mathbb{R}^3$ is the null vector. The absolute position and orientation of the object, $\mathbf{r}(t) \in \mathbb{R}^3$ and $\phi(t) \in \mathbb{R}^3$ respectively, can be written in compact form as $\mathbf{x} = [\mathbf{r}(t)|\phi(t)]^T \in \mathbb{R}^6$, such that $\mathbf{x} = \mathbf{k}(\mathbf{q}_r)$. The vector function $\mathbf{k}(\cdot) \in \mathbb{R}^6$ represents the robot direct kinematics. Similarly, the linear and angular absolute velocities of the object, $\dot{\mathbf{r}}(t) \in \mathbb{R}^3$ and $\omega(t) \in \mathbb{R}^3$ respectively, can be written in compact form as $\mathbf{v} = [\dot{\mathbf{r}}(t)|\omega(t)]^T \in \mathbb{R}^6$. In particular τ_{ri} , τ_{rc} , $\mathbf{J}_r^T \mathbf{h}_f$, $\mathbf{J}_r^T \mathbf{h}_c$ in \mathbb{R}^n represent respectively the portion of actuator torques which are used to counteract the manipulator own inertia, the manipulator own weight, the external wrenches due to object inertia and weight. For the purpose of the following sections, the term τ_{ri} is also expressed as:

$$\tau_{ri} = \dot{\mathbf{p}}_r(\mathbf{q}_r, \dot{\mathbf{q}}_r, \ddot{\mathbf{q}}_r) - \frac{1}{2} \left(\frac{\partial \mathbf{p}_r}{\partial \mathbf{q}_r} \right)^T \dot{\mathbf{q}}_r \quad (2)$$

where $\mathbf{p}_r(\mathbf{q}_r, \dot{\mathbf{q}}_r) \equiv \mathbf{M}_r(\mathbf{q}_r) \dot{\mathbf{q}}_r$ is the manipulator *generalized momentum* (see [22], pp. 143).

3.2. Background on parallel manipulators dynamic model

A typical PKM (a closed kinematic chain) is depicted in Fig. 2. In order to derive the PKM dynamic model, a possible approach is to consider a reduced system, i.e. a tree topology mechanism obtained by cutting the loops in a closed chain mechanism (see e.g. [24]). The dynamics of the reduced system (an open kinematic chain) can be described by an equation of the same form of Eq. (1) where, however, not all the pairs are actuated. The original (closed) and the reduced system are then assumed to experience the same external forces and to undergo the same motions. Let the closed chain consist of a total of k one d.o.f. joints, n of which are actuated. Let then define:

$$\Phi(\mathbf{q}_a) = \frac{\partial \mathbf{q}_r}{\partial \mathbf{q}_a} = \begin{bmatrix} \frac{\partial \mathbf{q}_{pr}}{\partial \mathbf{q}_a} \\ \mathbf{I}_n \end{bmatrix}, \quad \bar{\mathbf{V}} = \begin{bmatrix} \Phi^T \mathbf{V}_{1r}(\mathbf{q}_r) \Phi \\ \vdots \\ \Phi^T \mathbf{V}_{nr}(\mathbf{q}_r) \Phi \end{bmatrix}, \quad (3)$$

$$\mathbf{M}_1 = \Phi^T \mathbf{M}_r \Phi, \quad \mathbf{M}_2 = \Phi^T \mathbf{M}_r,$$

$$\mathbf{G} = \Phi^T \tau_{rc}, \quad \mathbf{J} = \mathbf{J}_r \Phi,$$

where the subscript r denotes quantities which refer to the reduced system dynamics (see. Eq. (1)), $\mathbf{q}_a \in \mathbb{R}^n$ and $\mathbf{q}_p \in \mathbb{R}^{k-n}$ are the position vectors of the actuated and passive joints respectively ($\tau_a \in \mathbb{R}^n$ and $\tau_p \in \mathbb{R}^{k-n}$ being the corresponding generalized force vectors), $\mathbf{q}_r = [\mathbf{q}_{pr}|\mathbf{q}_a]^T \in \mathbb{R}^m$ is the position vector of the reduced system, $\mathbf{q}_{pr} \subset \mathbf{q}_p$ is the subset of the passive joints' position vector that are also part of the reduced system, and $\Phi \in \mathbb{R}^{m \times n}$ is the *generalized actuating force transformation* [24]. Note that friction forces on passive joints, mainly due to sliding pairs, can be reasonably neglected with respect to friction forces within the actuator gear reducers. Therefore, similarly to [24], $\tau_p = \mathbf{0}$. In particular, in case

of pick-and-place operations, the vector of actuation torques, τ_a , can be expressed as:

$$\tau_a = \Phi^T \tau_r = \mathbf{M}_1(\mathbf{q}_a) \ddot{\mathbf{q}}_a + \mathbf{M}_2(\mathbf{q}_a) \dot{\Phi} \dot{\mathbf{q}}_a + (\mathbf{I}_n \otimes \dot{\mathbf{q}}_a^T) \bar{\mathbf{V}}(\mathbf{q}_a) \dot{\mathbf{q}}_a + \mathbf{G}(\mathbf{q}_a) + \mathbf{J}^T(\mathbf{q}_a) \mathbf{h} \quad (4)$$

Eq. (4) describes parallel manipulator dynamics away from actuator singularity. For the purpose of the calculations performed in Section 6, it is useful to highlight that the vector Φ is position dependent (i.e. $\Phi = \Phi(\mathbf{q}_a)$) and that Eq. (4) reduces to Eq. (1) whenever $\tau_r \equiv \tau_a$ (i.e. $\Phi = \mathbf{I}_n \Rightarrow \dot{\Phi} = \mathbf{0}$). Therefore, the energy saving method described in the following can be equally applied to both serial and parallel manipulators.

3.3. Actuation subsystem

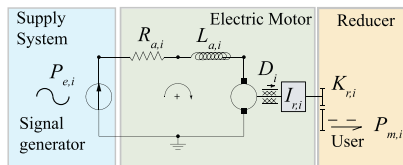
Fig. 4a shows a lumped-parameter model of a typical gear motor (position-controlled PM machine + speed reducer) which converts electrical power $P_{e,i}$ into mechanical power $P_{m,i}$. Let conventionally assume $P_{e,i} > 0$, $P_{m,i} > 0$ when the power flows from the converter to the electric machine and from the reducer output shaft to the user. The actuator can then function as either motor ($P_{e,i} > 0$ and $P_{m,i} > 0$), brake ($P_{e,i} > 0$ and $P_{m,i} < 0$) or generator ($P_{e,i} < 0$ and $P_{m,i} < 0$). In this latter condition, depending on the capabilities of the electronic driver, the negative electric power can be either dissipated as heat on a braking chopper (condition known as dynamic braking) or transferred back to the energy source (condition known as regenerative braking) which turns beneficial in terms of both efficiency and dynamic performance [22,25]. Commonly, a regenerative module which allows energy backflow is mounted on the AC/DC section of the converter.

Considering the overall robot actuation system, owing to the high dynamic demand, the PM machines are usually driven in regenerative mode by multidrive systems [17,26] comprising an energy source, a controllable power converter (AC/DC module + DC link + DC/AC modules) and a series of gear motors as schematized in Fig. 4b. In such a case, a common DC-Bus is used to supply several DC/AC modules that power the individual motor. The energy distribution over the common bus allows for motor-to-motor braking (energy exchange) possibly without the need for a braking chopper or a regenerative supply unit, see e.g. [27]. With reference to the lumped parameter model of the single motor depicted in Fig. 4a, the overall actuation subsystem dynamics (for n actuators) can be written as:

$$\mathbf{v}_a = \mathbf{R}_a \mathbf{i}_a + \mathbf{L}_a \dot{\mathbf{i}}_a + \mathbf{K}_v \mathbf{K}_r \dot{\mathbf{q}}_a \approx \mathbf{R}_a \mathbf{i}_a + \mathbf{K}_v \mathbf{K}_r \dot{\mathbf{q}}_a \quad (5)$$

$$\mathbf{I}_r \mathbf{K}_r \dot{\mathbf{q}}_a = \mathbf{K}_T \mathbf{i}_a - \mathbf{D} \mathbf{K}_r \dot{\mathbf{q}}_a - \mathbf{K}_r^{-1} \tau_a$$

where, for $j = 1 \dots n$, $\mathbf{v}_a = [v_{a,j}]$ and $\mathbf{i}_a = [i_{a,j}]$ are column vectors of the supplied armature voltages and currents respectively, $\mathbf{R}_a = \text{diag}\{R_{a,j}\}$, $\mathbf{L}_a = \text{diag}\{L_{a,j}\}$, $\mathbf{K}_v = \text{diag}\{K_{v,j}\}$, $\mathbf{K}_r = \text{diag}\{K_{r,j}\}$, $\mathbf{I}_r = \text{diag}\{I_{r,j}\}$,



(a) PM electric motor and speed reducer: lumped parameter model.

$\mathbf{K}_T = \text{diag}\{K_{T,j}\}$ and $\mathbf{D} = \text{diag}\{D_j\}$ are constant diagonal matrices of the different armature electric resistances, armature inductances, back emf constants, gear ratios, rotor inertias, motor torque constants, and viscous friction coefficients respectively. Note that $K_{T,i}/K_{v,i} \approx 1$ for trapezoidal type AC brushless [9]. In addition, concerning servomotors commonly used in robotic applications, the armature inductance $L_{a,i}$ can be neglected and the mechanical viscous friction coefficient is negligible with respect to the electrical friction coefficient ($R_{a,i} \gg D_i$).

4. Calculation of the total power and energy consumption

In this section, the manipulator power consumption is calculated on the basis of the following assumptions (recalled for clarity):

- The PM machines' inductances, \mathbf{L}_a , are neglected.
- Regenerative motor braking is assumed at all times.
- The mechanical losses are concentrated in the gear reducers only (i.e. the losses in the passive kinematic pairs are neglected).
- The mechanical frictions are modeled via constant viscous terms, \mathbf{D} .

Hence, concerning both actuator and robot dynamics (Fig. 2), the total instantaneous power, P_e , supplied to the manipulator is given by:

$$P_e = \mathbf{i}_a^T \mathbf{v}_a = \mathbf{i}_a^T \mathbf{R}_a \mathbf{i}_a + \mathbf{i}_a^T \mathbf{K}_v \mathbf{K}_r \dot{\mathbf{q}}_a \quad (6)$$

The armature current vector is found from Eq. (5):

$$\mathbf{i}_a = \mathbf{K}_T^{-1} \mathbf{K}_r^{-1} \tau + \mathbf{K}_T^{-1} \mathbf{K}_r \mathbf{D} \dot{\mathbf{q}}_a \quad (7)$$

where

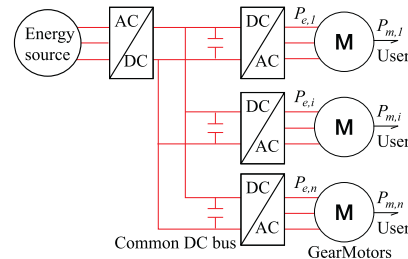
$$\tau = (\tau_l + \mathbf{G}) + (\mathbf{J}^T \mathbf{h}_l + \mathbf{J}^T \mathbf{h}_g) \quad (8)$$

$$\tau_l = [\mathbf{M}_1 + \mathbf{K}_T^T \mathbf{I}_r] \ddot{\mathbf{q}}_a + [\mathbf{M}_2 \dot{\Phi} + (\mathbf{I}_n \otimes \dot{\mathbf{q}}_a^T) \bar{\mathbf{V}}] \dot{\mathbf{q}}_a$$

Differently from τ_a (see Eq. (4)), the torque vector τ includes the inertial effects due to the rotor inertias $I_{r,i}$. Note that, in Eq. (8), it is convenient to split the torque contributions due to the inertia and weight of payload ($\mathbf{J}^T \mathbf{h}_l$ and $\mathbf{J}^T \mathbf{h}_g$, respectively) or manipulator (τ_l and \mathbf{G} , respectively). By introducing Eq. (7) in Eq. (6), the following expression can be found:

$$P_e = \tau^T \mathbf{R}_a (\mathbf{K}_r \mathbf{K}_T)^{-2} \tau + \tau^T \mathbf{K}_T^{-1} \mathbf{K}_v \mathbf{K}_r \dot{\mathbf{q}}_a + 2 \tau^T \mathbf{R}_a \mathbf{K}_T^{-2} \mathbf{D} \dot{\mathbf{q}}_a + \dot{\mathbf{q}}_a^T (\mathbf{R}_a \mathbf{K}_T^{-2} \mathbf{K}_r^2 \mathbf{D}^2 + \mathbf{K}_v \mathbf{K}_T^{-1} \mathbf{K}_r^2 \mathbf{D}) \dot{\mathbf{q}}_a \quad (9)$$

where, assuming the actuators being trapezoidal type AC brushless, $\mathbf{K}_T^{-1} \mathbf{K}_v = \mathbf{I}_n$ [9]. Eq. (9) can be denoted as:



(b) Schematic of a multidrive system for industrial applications.

Fig. 4. Electromechanical model of a PM electric gearmotor (a) and multidrive system schematic (b).

$$P = \boldsymbol{\tau}^T \mathbf{R}_1 \boldsymbol{\tau} + \boldsymbol{\tau}^T \mathbf{R}_2 \dot{\mathbf{q}}_a + \dot{\mathbf{q}}_a^T \mathbf{R}_3 \dot{\mathbf{q}}_a + \boldsymbol{\tau}^T \dot{\mathbf{q}}_a \quad (10)$$

having defined the following matrices:

$$\begin{aligned} \mathbf{R}_1 &= \mathbf{R}_a (\mathbf{K}_r \mathbf{K}_T)^{-2} \\ \mathbf{R}_2 &= 2\mathbf{R}_a \mathbf{K}_T^{-2} \mathbf{D} \\ \mathbf{R}_3 &= \mathbf{R}_a \mathbf{K}_T^{-2} \mathbf{K}_r^2 \mathbf{D}^2 + \mathbf{K}_v \mathbf{K}_T^{-1} \mathbf{K}_r^2 \mathbf{D} \end{aligned} \quad (11)$$

The power flow can then be numerically computed by knowing the mechanical (inertia, viscous friction, gear ratio) and electrical (armature resistance and inductance) system parameters. Nonetheless, in general, the mechanical dissipations (viscous friction coefficients, D_i) are negligible with respect to the electrical dissipations (armature resistance, $R_{a,i}$) [28]. Assuming $\mathbf{D} \approx \mathbf{0}$, the power consumption can be simplified as:

$$P = \boldsymbol{\tau}^T \mathbf{R}_1 \boldsymbol{\tau} + \boldsymbol{\tau}^T \dot{\mathbf{q}}_a \quad (12)$$

As for the energy necessary to perform a given operation, over the time period $t \in [0, T_f]$, it is given by the time integral of Eq. (9). In particular, by recalling the partitioning of the loading torques introduced in Eq. (8), the overall energy flow can be expressed as:

$$E = E_d + E_{km} + E_{gm} + E_{kl} + E_{gl} \quad (13)$$

where

$$\begin{aligned} E_d &= \int_0^{T_f} [\boldsymbol{\tau}^T \mathbf{R}_1 \boldsymbol{\tau} + \boldsymbol{\tau}^T \mathbf{R}_2 \dot{\mathbf{q}}_a + \dot{\mathbf{q}}_a^T \mathbf{R}_3 \dot{\mathbf{q}}_a] dt \\ E_{km} &= \int_0^{T_f} \boldsymbol{\tau}_l^T \dot{\mathbf{q}}_a dt \\ E_{gm} &= \int_0^{T_f} \mathbf{G}^T \dot{\mathbf{q}}_a dt \\ E_{kl} &= \int_0^{T_f} [\mathbf{J}^T \mathbf{h}_l]^T \dot{\mathbf{q}}_a dt = \int_0^{T_f} \mathbf{h}_l^T \mathbf{v} dt \\ E_{gl} &= \int_0^{T_f} [\mathbf{J}^T \mathbf{h}_g]^T \dot{\mathbf{q}}_a dt = \int_0^{T_f} \mathbf{h}_g^T \mathbf{v} dt \end{aligned} \quad (14)$$

Owing the servoactuator model of Eq. (5), the aforementioned formulation for the energy contributions can be interpreted as follows:

- E_d , which is function of the overall torque vector $\boldsymbol{\tau}$, is the energy dissipated through the armature resistance and through mechanical viscous friction.
- E_{km} , which is function of the inertial torque vector $\boldsymbol{\tau}_l$, is the kinetic energy stored in the manipulator inertial field.
- E_{gm} is the gravitational potential energy due to the manipulator masses.
- E_{kl} , which can be written as function of \mathbf{v} and \mathbf{h}_l , is the kinetic energy delivered to the user. In case of pick-and-place operations where a workpiece is picked up and delivered at zero velocity, $E_{kl} = 0$.
- E_{gl} , which can be written as function of \mathbf{v} and \mathbf{h}_g , is the variation of the workpiece potential energy.

5. Power consumption during cyclic pick-and-place operations

Recalling the schematic depicted in Fig. 1a, suppose that the robot end effector executes cyclic pick-and-place operations for $t \in [0, T_0]$ whereas it is kept stationary, in a configuration $\mathbf{q}_a(T_0)$, for $t \in [T_0, T_f]$. Suppose the handled object is carried for $t \in [T_A, T_B] \subset [0, T_0]$, and it is picked up and delivered at zero velocity $\mathbf{v}(T_A) = \mathbf{v}(T_B) = \mathbf{0}$. In this case, under the assumptions recalled in the previous section, it is useful to highlight that the overall energy consumption is simply given by:

$$E = E_d + E_{gl} \quad (15)$$

In fact, considering a manipulator which starts its motion at $t = 0$ in a given configuration and ends its motion at $t = T_f$ in that same configuration, it is easily proven that $E_{km} = E_{gm} = 0$.

As for the manipulator kinetic energy, resorting to Eqs. (2) and (4)

$$\begin{aligned} E_{km} &= \int_0^{T_f} \boldsymbol{\tau}_l^T \dot{\mathbf{q}}_a dt = \int_0^{T_f} (\boldsymbol{\Phi}^T \boldsymbol{\tau}_{rl})^T (\boldsymbol{\Phi}^{-1} \dot{\mathbf{q}}_r) dt \\ &= \int_0^{T_f} \left[\dot{\mathbf{p}}_r - \frac{1}{2} \left(\frac{\partial \mathbf{p}_r}{\partial \dot{\mathbf{q}}_r} \right)^T \dot{\mathbf{q}}_r \right]^T \dot{\mathbf{q}}_r dt \\ &= \int_0^{T_f} \left[\dot{\mathbf{p}}_r^T \dot{\mathbf{q}}_r - \frac{1}{2} \dot{\mathbf{q}}_r^T \left(\frac{\partial \mathbf{p}_r}{\partial \dot{\mathbf{q}}_r} \right)^T \dot{\mathbf{q}}_r \right] dt = \int_0^{T_f} \frac{1}{2} \dot{\mathbf{q}}_r^T \dot{\mathbf{p}}_r dt \\ &= \frac{1}{2} \int_{\mathbf{p}_0}^{\mathbf{p}_F} \dot{\mathbf{q}}_r^T d\mathbf{p}_r = 0 \end{aligned} \quad (16)$$

where \mathbf{p}_0 and \mathbf{p}_F are the reduced system generalized momenta calculated at $t = 0$ and $t = T_f$ respectively. According to the definition of manipulator generalized momentum (see Section 3.1), $\mathbf{p}_0 = \mathbf{p}_F = \mathbf{0}$.

As for the manipulator potential energy, resorting to Eqs. (1) and (4)

$$\begin{aligned} E_{gm} &= \int_0^{T_f} \mathbf{G}^T \dot{\mathbf{q}}_a dt = \int_0^{T_f} (\boldsymbol{\Phi}^T \boldsymbol{\tau}_{rg})^T (\boldsymbol{\Phi}^{-1} \dot{\mathbf{q}}_r) dt \\ &= \int_{\mathbf{q}_r(0)}^{\mathbf{q}_r(T_f)} dH_r(\mathbf{q}_r) = 0 \end{aligned} \quad (17)$$

Supposing that Eq. (12) holds (i.e. $\mathbf{D} \approx \mathbf{0}$) and denoting $\Delta T_{FO} = T_f - T_0$, the energy consumption for $t \in [T_0, T_f]$ is then given by:

$$E = \mathbf{G}^T(\mathbf{q}_a(T_0)) \mathbf{R}_1 \mathbf{G}(\mathbf{q}_a(T_0)) \Delta T_{FO} \quad (18)$$

as long as the joints velocities are null (i.e. $\dot{\mathbf{q}}_a = 0$) within the considered time frame. Therefore, the total EC for $t \in [0, T_f]$ is finally given by:

$$E - E_l = \int_0^{T_0} \boldsymbol{\tau}^T \mathbf{R}_1 \boldsymbol{\tau} dt + \mathbf{G}^T(\mathbf{q}_a(T_0)) \mathbf{R}_1 \mathbf{G}(\mathbf{q}_a(T_0)) \Delta T_{FO} \quad (19)$$

Eq. (8) might then be introduced into Eq. (19) in order to better highlight the contribution of purely inertial and gravitational loads. In particular, let first discard gravitational loads. In this case, recalling that the object is picked up and delivered at zero velocity, the terms E_{gl}, E_{kl} are null (i.e. the mechanical work supplied to the user is null). On the other hand, the terms $\boldsymbol{\tau}_l$ and $\mathbf{J}^T \mathbf{h}_l$ increase for increasing joint velocities and accelerations (see Eqs. (8) and (1) respectively) and vanishes when the robot is stationary. Therefore, it is possible to conclude that, when the cycle time approaches infinity, the overall EC approaches zero and can be trivially decreased by simply slowing down the motions (see Fig. 5, red¹ dash-dot line). On the other hand, if only gravitational torques are considered, the EC becomes a monotonically increasing function of TET (see Fig. 5, black continuous line). Hence, in real conditions ($\mathbf{G} \neq \mathbf{0}$), the total EC is given by the combination of two monotonic functions with opposite trends, highlighting that there may exist a minimum for some value of TET (as shown in Fig. 1b and in Fig. 5, dash blue line).

6. Trajectory time scaling applied to energy consumption minimization

As previously mentioned, many scheduling approaches [16,29], assume each robot operating at its maximum achievable speed along given paths (hereafter taken as reference path). In this case,

¹ For interpretation of color in Fig. 5, the reader is referred to the web version of this article.

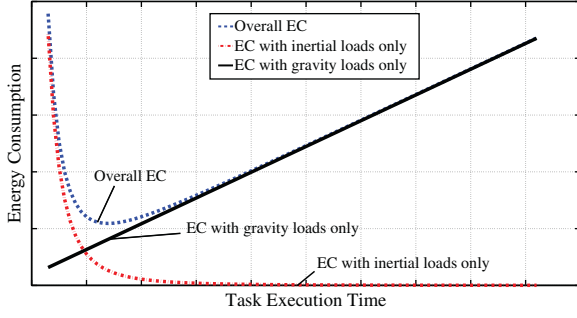


Fig. 5. Qualitative plots of EC in pick-and-place operations. Overall EC, contribution of inertial loads, contribution of gravity loads.

the desired position profile in the joint space is completed within $t \in [0, T_0]$, T_0 being the minimum possible TET. The corresponding active joint trajectory, $\mathbf{q}_0(t)$, $\dot{\mathbf{q}}_0(t)$, $\ddot{\mathbf{q}}_0(t)$, is referred to as reference trajectory. In the following, all quantities referring to this reference trajectory will be denoted with O subscript. After the path completion, the robots are often kept stationary up to time T_F (i.e. for the time period ΔT_{FO}), waiting for other robots to complete their operations. The overall EC is therefore given by Eq. (19). In this situation, which happens very frequently in practice, it is possible to re-program the manipulator in order to achieve an energy-optimal motion while maintaining the same TCP position profile. Suppose that the aforementioned reference path is followed with a trajectory whose position profile is given by:

$$\mathbf{q}_s(t) = \mathbf{q}_0(\alpha^{-1}t) \quad (20)$$

where $\alpha \geq 1$ is denoted as *scaling factor*. In the following, all quantities referring to this scaled trajectory will be denoted with s subscript. Let then calculate how the overall EC vary with respect to α when Eq. (20) is applied to the robot dynamics.

In particular, defining a scaled time frame as $t' = \alpha^{-1}t$, $t' \in [0, T_F]$, the scaled trajectory is given by:

$$\begin{aligned} \mathbf{q}_s(t) &= \mathbf{q}_0(t') \\ \dot{\mathbf{q}}_s(t) &= \frac{d\mathbf{q}_0(t')}{\alpha dt'} = \alpha^{-1}\dot{\mathbf{q}}_0(t') \\ \ddot{\mathbf{q}}_s(t) &= \frac{d(\alpha^{-1}\dot{\mathbf{q}}_0(t'))}{\alpha dt'} = \alpha^{-2}\ddot{\mathbf{q}}_0(t') \end{aligned} \quad (21)$$

Naturally, being position dependent, both the TCP path, $\mathbf{x}_s = \mathbf{k}(\mathbf{q}_s)$, and the generalized actuating force transformation, $\Phi_s(\mathbf{q}_s)$, remains unaltered after time scaling (i.e. $[\mathbf{r}_s(t)|\phi_s(t)]^T = [\mathbf{r}_0(t')|\phi_0(t')]^T$ and $\Phi_s(t) = \Phi_0(t')$), such that their time derivative is given by:

$$\mathbf{v}_s(t) = \frac{d\mathbf{x}_0(t')}{\alpha dt'} = \alpha^{-1}\mathbf{v}_0(t') \quad \dot{\Phi}_s(t) = \frac{d\Phi_0(t')}{\alpha dt'} = \alpha^{-1}\dot{\Phi}_0(t') \quad (22)$$

In the same manner, the scaled object equation of motion is given by:

$$\mathbf{h}_s(t) = \alpha^{-2} \left[\mathfrak{I}\dot{\omega}_0(t') + \omega_0(t') \times \mathfrak{I}\omega_0(t') \right] + \begin{bmatrix} m\ddot{\mathbf{r}}_0(t') \\ m\mathbf{g} \\ \mathbf{0} \end{bmatrix} = \alpha^{-2}\mathbf{h}_{10}(t') + \mathbf{h}_{g0}(t') \quad (23)$$

As for the motor torques, their dependency on \mathbf{q}_0 , $\dot{\mathbf{q}}_0$, $\ddot{\mathbf{q}}_0$, and $\dot{\Phi}_0$ has been highlighted in Eq. (4), such that the scaled torques can be computed as:

$$\begin{aligned} \boldsymbol{\tau}_s &= \mathbf{M}_1(\mathbf{q}_s(t))\ddot{\mathbf{q}}_s(t) + \mathbf{M}_2(\mathbf{q}_s(t))\dot{\Phi}_s(t)\dot{\mathbf{q}}_s(t) + (\mathbf{I}_n \\ &\quad \otimes \dot{\mathbf{q}}_s^T(t))\mathbf{V}(\mathbf{q}_s(t))\dot{\mathbf{q}}_s(t) + \mathbf{G}(\mathbf{q}_s(t)) + \mathbf{J}^T(\mathbf{q}_s(t))\mathbf{h}_s(t) \end{aligned} \quad (24)$$

Hence, recalling the notation defined in Eq. (8), and introducing Eqs. (21)–(23) into Eq. (24), the scaled torques can be written as:

$$\boldsymbol{\tau}_s(t) = \alpha^{-2} \left(\boldsymbol{\tau}_{10}(t') + \mathbf{J}_0^T(t')\mathbf{h}_{10}(t') \right) + \left(\mathbf{G}_0(t') + \mathbf{J}_0^T(t')\mathbf{h}_{g0}(t') \right) \quad (25)$$

This same equation highlights that the scaling procedure alters the inertial torques by a factor equalling α^{-2} whereas the gravitational torques remain unaltered. Note that the presence of the generalized actuating force transformation Φ , and its time derivative is the main difference between serial and parallel robot dynamics.

The power input associated with the scaled trajectory is found by introducing Eqs. (21) and (25) into Eq. (10) as written with respect to the scaled trajectory. The following expression is found:

$$P_s(t) = \boldsymbol{\tau}_s^T \mathbf{R}_1 \boldsymbol{\tau}_s + \dot{\mathbf{q}}_s^T \mathbf{R}_2 \dot{\mathbf{q}}_s + \ddot{\mathbf{q}}_s^T \mathbf{R}_3 \ddot{\mathbf{q}}_s + \dot{\Phi}_s^T \dot{\mathbf{q}}_s = \sum_{i=0}^4 \alpha^{-i} p_i(t') \quad (26)$$

where

$$\begin{aligned} p_4 &= \boldsymbol{\tau}_{10}^T(t') \mathbf{R}_1 \boldsymbol{\tau}_{10}(t') \\ p_3 &= \dot{\mathbf{q}}_{10}^T(t') (\mathbf{R}_2 - \mathbf{I}_n) \dot{\mathbf{q}}_{10}(t') \\ p_2 &= 2\dot{\mathbf{q}}_{10}^T(t') \mathbf{R}_1 \bar{\mathbf{G}}_0(\mathbf{q}_0(t')) + \ddot{\mathbf{q}}_{10}^T(t') \mathbf{R}_3 \ddot{\mathbf{q}}_{10}(t') \\ p_1 &= \bar{\mathbf{G}}_0^T(\mathbf{q}_0(t')) (\mathbf{R}_2 - \mathbf{I}_n) \dot{\mathbf{q}}_{10}(t') \\ p_0 &= \bar{\mathbf{G}}_0^T(\mathbf{q}_0(t')) \mathbf{R}_1 \bar{\mathbf{G}}_0(\mathbf{q}_0(t')) \\ \bar{\boldsymbol{\tau}}_{10} &= \boldsymbol{\tau}_{10} + \mathbf{J}_0^T(t') \mathbf{h}_{10} \\ \bar{\mathbf{G}}_0 &= \mathbf{G}_0 + \mathbf{J}_0^T(t') \mathbf{h}_{g0} \end{aligned} \quad (27)$$

Given the power consumption concerning the scaled trajectory, the overall EC can be computed as:

$$\begin{aligned} E_s(t) &= \int_0^{T_F} P_s(t) dt = \int_0^{T_0} P_s(t') \alpha dt' = \sum_{i=0}^4 \alpha^{1-i} \int_0^{T_0} p_i(t') dt' \\ &= T_0 \sum_{i=0}^4 \alpha^{1-i} \bar{p}_i(t') \end{aligned} \quad (28)$$

where $\bar{p}_i(t') = T_0^{-1} \int_0^{T_0} p_i(t') dt'$, $i = 1 \dots 4$, are mean powers due to the various contributions highlighted in Eq. (26). Note the change of integration variable in Eq. (28) as $t = \alpha t'$. In particular, these terms depend on the model electromechanical parameters, \mathbf{R}_1 , \mathbf{R}_2 , \mathbf{R}_3 , and on the reference joint trajectory and torques. Hence, supposing the overall energy input along the reference trajectory as given, the useful result highlighted by Eq. (28) is that the EC concerning the scaled trajectory can be computed as a fifth order power series in the scaling factor α .

6.1. Evaluation of the method's efficacy

The efficacy of the proposed scaling method can be computed by means of the following EC ratio:

$$\eta_{EC} = 1 - \frac{E_s - E_l}{E_0 - E_l} \quad (29)$$

where E_s and E_0 are the EC related to the scaled and reference trajectory respectively. In particular, the energy E_0 is found by setting $\alpha = 1$ in Eq. (28) whereas E_l , being the potential energy delivered to the user, remains unaltered after time-scaling. The term η_{EC} simply defines the relative ratio between the dissipated electric energies (i.e. the difference between the total EC and the energy delivered to the user) in the case of reference and energy-optimal operations. Considering once again a robot performing a pick-and-place operation for $t \in [0, T_0]$ and kept stationary for $t \in [T_0, T_F]$, and by neglecting mechanical viscous friction ($\mathbf{D} \approx \mathbf{0}$), the efficiency ratio may be computed as:

$$\tilde{\eta}_{EC} = 1 - \frac{\int_0^{T_F} \boldsymbol{\tau}_s^T \mathbf{R}_1 \boldsymbol{\tau}_s dt}{\int_0^{T_0} \boldsymbol{\tau}_0^T \mathbf{R}_1 \boldsymbol{\tau}_0 dt + \mathbf{G}^T(\mathbf{q}_0(T_0)) \mathbf{R}_1 \mathbf{G}(\mathbf{q}_0(T_0)) \Delta T_{FO}} \quad (30)$$

Note that Eq. (30) simplifies whenever the robot actuators are equal, as it generally happens in parallel manipulators. In such a case, the contribution of the matrix \mathbf{R}_1 disappears, the efficiency ratio becoming independent of the actuator system parameters (i.e. stator resistance $R_{a,i}$, equivalent torque constant $K_{T,i}$, gear ratio $K_{r,i}$):

$$\hat{\eta}_{EC} = 1 - \frac{\int_0^{T_F} \boldsymbol{\tau}_s^T \boldsymbol{\tau}_s dt}{\int_0^{T_0} \boldsymbol{\tau}_0^T \boldsymbol{\tau}_0 dt + \mathbf{G}^T(\mathbf{q}_0(T_0))\mathbf{G}(\mathbf{q}_0(T_0))\Delta T_{FO}} \quad (31)$$

The simplified Eq. (31) turns particularly useful when the model electromechanical parameters are not accessible by the end user for confidentiality reasons. In such a case, the robot masses and inertias can be determined by means of well known identification techniques (e.g. [30]). On the other hand, the determination of the actuator parameters is challenging and results are usually affected by large errors (especially for what concerns the value of the motors' resistances [31]).

At last, recalling the schematic depicted in Fig. 1a, it should be highlighted that the scaling procedure might be easily restricted to those time intervals along which the manipulator is not carrying any payload (i.e. for $t \in [T_B, T_{A2}]$) or simply to the homing motions (i.e. for $t \in [T_A, T_F]$).

7. Simulation case studies

Two case studies are simulated in order to assess the validity of the proposed method in the case of serial and parallel robots.

First, a PUMA 560 anthropomorphic arm performs cyclic pick-and-place operations following a 3D cubic spline. With reference to Fig. 6, an object with mass $m = 2$ kg is initially still, it is then grabbed from its resting position (point A) and finally delivered at null velocity in a different position (point B). The spline control points, expressed with respect to a fixed coordinate system whose origin lies on the manipulator TCP at time $t = 0$ (Fig. 6), are reported in Table 1.

The robot electromechanical parameters (including friction coefficients) are taken from [32,14]. The reference TET is $T_0 = 4$ s, the overall cycle time is $T_F = 12$ s, whereas the reference joint space trajectory $\mathbf{q}_0(t)$, $\dot{\mathbf{q}}_0(t)$, $\ddot{\mathbf{q}}_0(t)$, and torques $\boldsymbol{\tau}_0(t)$ are found by means of RecurDyn multibody software [33]. As an example, the position and torque profiles of the first three joints of the manipulator are reported in Figs. 7 and 8, the profiles concerning the wrist joints being omitted for clarity. In any case, the first three joints are

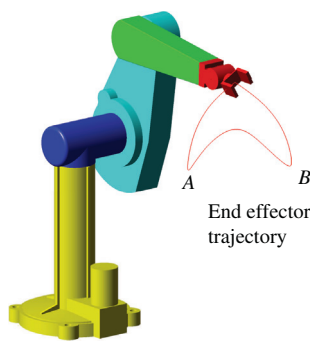


Fig. 6. PUMA arm 3D schematic and end-effector trajectory.

Table 1
Coordinates of the control points of the spline path.

Point	1	2	3	4	5	6	7	8	9
x (mm)	0	190.53	190.53	170.53	90.26	10.00	0	0	0
y (mm)	0	110.00	110.00	75.36	-63.66	-202.68	-220.00	-220.00	0
z (mm)	0	-250.00	-300.00	-275.00	-150.00	-275.00	-300.00	-250.00	0

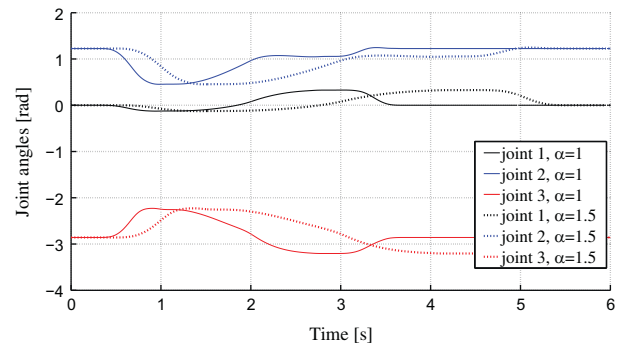


Fig. 7. Reference joint angles, $\alpha = 1$, and scaled joint space angles, $\alpha = 1.5$ for PUMA arm performing pick-and-place operations.

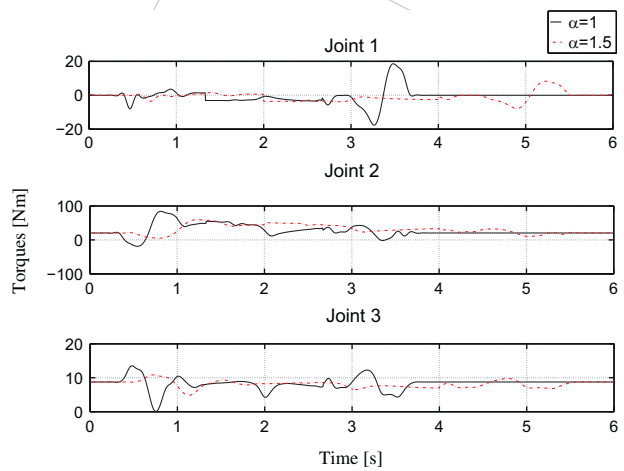


Fig. 8. Joint torques corresponding to the reference trajectory, $\alpha = 1$, and to the scaled trajectory, $\alpha = 1.5$.

charged with a higher EC when compared to the wrist joints which are used to simply orient the workpiece and are equipped with electric motors of smaller size. Figs. 7 and 8 also report the effect of the trajectory scaling by means of a constant scaling factor, $\alpha = 1.5$, as described in Eq. (20). At last, Fig. 9 depicts the EC as a function of the scaling factor α (continuous line) and accounts for the contribution of all the six robot joints. The EC presents a local minimum, \bar{E} , achieved for $\alpha = 1.55$, the corresponding relative EC ratio (see Eq. (29)) being $\eta_{EC} = 7.73\%$. Note that the TET equals the cycle time for $\alpha = 3$. In addition, the same figure reports the EC profile in case of absence of frictional and gravitational load respectively. In the latter a case, the EC is a monotonic function decreasing for increasing scaling factor (i.e. slowing down the operation). By neglecting the contribution of viscous friction ($\mathbf{D} = \mathbf{0}$), the simplified Eqs. (12) and (30) can be applied resulting in an optimal scaling factor $\tilde{\alpha} = 1.50$ and relative EC ratio $\tilde{\eta}_{EC} = 7.71\%$.

As a second case study, the PKM depicted in Fig. 10 performs the same pick-and-place operations reported in the previous example.

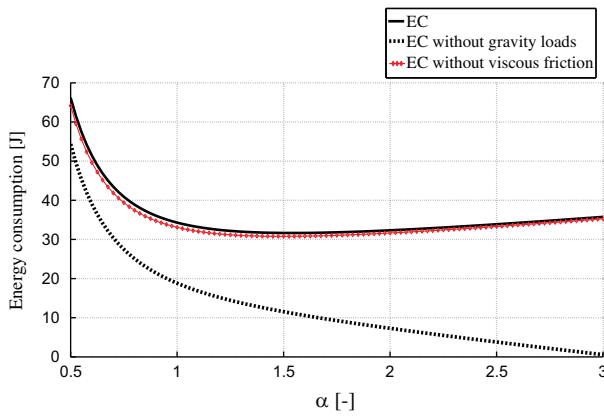


Fig. 9. Energy consumption as a function of scaling factor α in case of complete electromechanical model, absence of viscous friction, and absence of gravity.

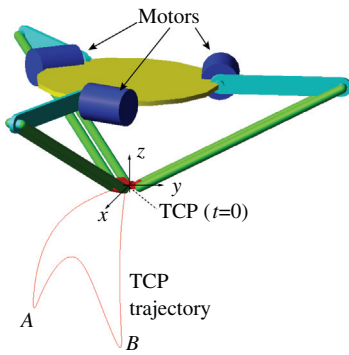


Fig. 10. PKM 3D schematic and end-effector trajectory.

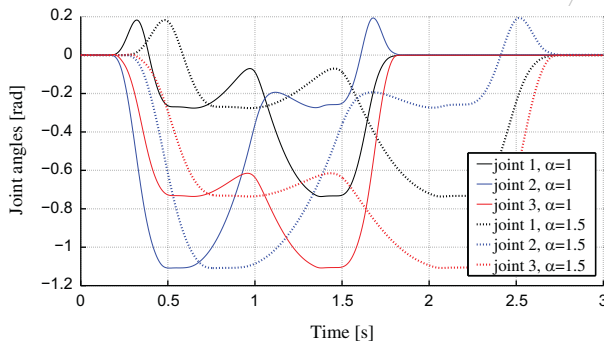


Fig. 11. Reference joint angles, $\alpha = 1$, and scaled joint space angles, $\alpha = 1.5$ for PKM performing pick-and-place operations.

The PKM dimensions and inertial parameters are taken from [34] whereas, for $j = 1, 3$, $R_{a_j} = 2.27 \Omega$, $K_{r_j} = 15$, $I_{r_j} = 3.0 \times 10^{-4} \text{ kg m}^2$. In particular, the gear motors parameters are selected according to the procedure described in [35] accounting for a transmission mean efficiency $\eta_r = 90 \%$ (i.e. $\tau_f = (\eta_r^{-1} - 1)\tau$). The reference TET is now $T_O = 2.0 \text{ s}$ and the overall cycle time is $T_F = 6.0 \text{ s}$. The simulated position and torque profiles of the three motors are reported in Figs. 11 and 12 for $\alpha = 1$ and $\alpha = 1.5$ respectively. The overall EC is depicted in Fig. 13 and presents a local minimum, \bar{E} , achieved for $\bar{\alpha} = 1.47$. The corresponding relative EC ratio is $\eta_{EC} = 9.84\%$. Once again, the TET equals the cycle time for $\alpha = 3$. By neglecting the friction contribution, an optimal scaling factor $\tilde{\alpha} = 1.35$ is found, the relative EC ratio being $\tilde{\eta}_{EC} = \tilde{\eta}_{EC} = 9.46\%$.

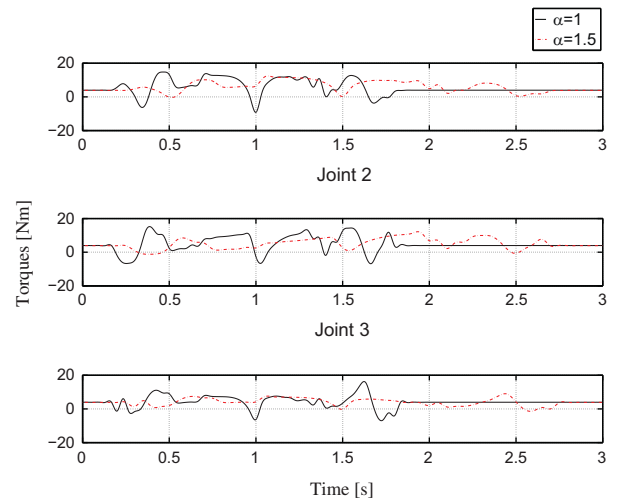


Fig. 12. Joint torque corresponding to the reference trajectory, $\alpha = 1$, and to the scaled trajectory, $\alpha = 1.5$. Simulation results.

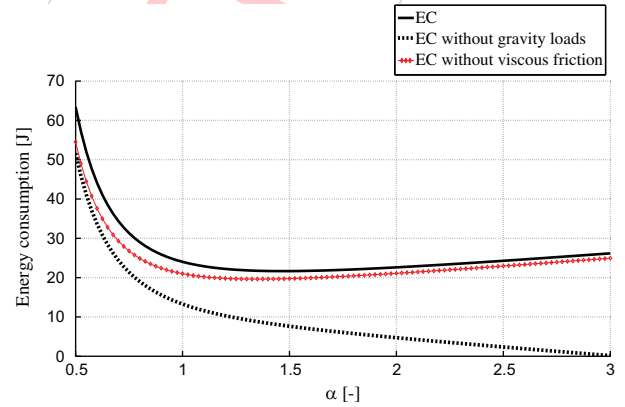


Fig. 13. Energy consumption as a function of scaling factor α in case of complete electromechanical model and absence of gravity. Simulation results.

8. Discussion and conclusions

A method for the energy consumption optimization of robotic systems has been presented. Differently from other optimization routines, the proposed strategy does not rely on either equipment replacement, plant modification or path re-planning. In fact, starting from given manipulator electromechanical parameters and pre-scheduled trajectories compatible with the actuation limits, an energy-optimal trajectory is simply determined by means of time-scaling.

After the presentation of preliminary experimental results and background theory, the different contributions of inertial, gravitational and dissipative energy terms are highlighted with respect to reference and scaled trajectories. Then, the approach has been tested on common parallel and serial robots performing cyclic pick-and-place operations. The results allow the operator to parameterize and adjust the manipulator operations in order to reduce the EC, whenever allowed by other scheduling constraints (e.g. during the homing motions). In particular, it has been recalled that slowing down an operation as much as possible is not always beneficial. In addition, it has been highlighted that the EC of a given operation as a function of the task execution time can be described by a fifth order power series. Regardless the robot topology, this information turns useful also when programming real industrial robots whose instantaneous powers can be derived by means of

black-box proprietary software (e.g. [36] where the robot inertial parameters are unavailable to the end-user). Future work includes a further improvement of the motor model, an experimental campaign to evaluate the method accuracy and efficacy on multi-robot cells (similarly to [37]), the development of on-line programming algorithms, and the implementation of dedicated simulation tools to be integrated on proprietary software.

References

- [1] ManuFuture. Strategic research agenda. Report of the high level group. ManuFuture Platform; 2006.
- [2] Menanteau P, Finon D, Lamy M. Prices versus quantities: choosing policies for promoting the development of renewable energy. *Energy Policy* 2003;31:799–812.
- [3] Hirzinger G et al. On a new generation of torque controlled light-weight robots. In: Proceedings of the IEEE international conference on robotics and automation; 2001. p. 3356–63.
- [4] Saidur R. A review on electrical motors energy use and energy savings. *Renew Sust Energy Rev* 2010;14:877–98.
- [5] Maimon O, Profeta E, Singer S. Energy analysis of robot task motions. *J Intell Robot Syst* 1991;4:175–98.
- [6] Vukobratovic M, Kircanski M. A method for optimal synthesis of manipulation robot trajectories. *ASME J Dynam Syst Meas Control* 1982;104(2):188–93.
- [7] Tan H, Potts R. Discrete trajectory planner for robotic arms with six degrees of freedom. *IEEE Trans Robot Autom* 1989;5(5):681–90.
- [8] Diken H. Energy efficient sinusoidal path planning of robot manipulators. *Mech Mach Theory* 1994;29(6):785–92.
- [9] Park J. Motion profile planning of repetitive point-to-point control for maximum energy conversion under acceleration conditions. *Mechatronics* 2006;6(6):649–63.
- [10] Sergaki E, Stavrakakis G, Pouliezios A. Optimal robot speed trajectory by minimization of the actuator motor electromechanical losses. *J Intell Robot Syst* 2002;33:187–207.
- [11] Kim CH, Kim BK. Minimum-energy motion planning for differential-driven wheeled mobile robots. Motion planning. InTech; 2008. p. 192–226. ISBN: 978-953-7619-01-5.
- [12] Abba G, Chaillet N. Robot dynamic modeling using a power flow approach with application to biped locomotion. *Autonom Robots* 1999;6: 39–2.
- [13] Izumi T, Zhou H, Li Z. Optimal design of gear ratios and offset for energy conservation of an articulated manipulator. *IEEE Trans Autom Sci Eng* 2006;6(3):551–7.
- [14] Meyer N, Angeles J. Minimization of power losses in cooperating manipulators. In: American control conference; 1991. p. 3044–9.
- [15] Vergnano A, Thorstensson C, Lennartson B, Falkman P, Pellicciari M, Leali F, et al. Modeling and optimization of energy consumption in cooperative multi-robot systems. *IEEE Trans Autom Sci Eng* 2012;9(2):423–8.
- [16] Bobrow J, Dubowsky S, Gibson J. Time- optimal control of robotic manipulators along specified paths. *Int J Robot Res* 1985;4(3):3–17.
- [17] Meike D, Ribickis L. Energy efficient use of robotics in the automobile industry. In: ICAR international conference on advanced robotics; 2011. p. 507–11.
- [18] Moon S, Ahmad S. Time scaling of cooperative multirobot trajectories. *IEEE Trans Syst Man Cybernet* 1991;21(4):900–8.
- [19] Wigstrom O, Lennartson B, Vergnano A, Breitholtz C. High-level scheduling of energy optimal trajectories. *IEEE Trans Autom Sci Eng* 2012(99):1–8.
- [20] Guardabrazo T, de Santos PG. Building an energetic model to evaluate and optimize power consumption in walking robot. *Indus Robot* 2004;31(2):201–8.
- [21] Kolibal Z, Smetanova A. Experimental implementation of energy optimization by robot movement. In: IEEE 19th international workshop on robotics; 2010. p. 333–9.
- [22] Lewis FL, Abdallah CT, Dawson DM. Control of robot manipulators: theory and practice. New York: Marcel Dekker, Inc.; 2004.
- [23] Craig J. Introduction to robotics: mechanics and control. 3rd ed. Addison-Wesley Publishing Company, Inc.; 2005.
- [24] Park FC, Choi J, Ploen SR. Symbolic formulation of closed chain dynamics in independent coordinates. *Mech Mach Theory* 1999;34(5):731–51.
- [25] Hughes A. Electric motors and drives fundamentals, types and applications. London: Elsevier; 2006.
- [26] Aalto H. Multi-axis servo and system drives comparison. PhD thesis. Bachelor thesis. Metropolia: University of Applied Sciences; 2011.
- [27] ABB Robotics. Abb industrial drives, technical catalogue. ACS800_multidrive_revB_LR.pdf. <<http://www.abb.com>>.
- [28] Sciavicco L, Siciliano B, Villani L, Oriolo G. Robotics: modelling, planning and control. London: Springer; 2009.
- [29] Verscheure D, Diehl M, Schutter JD, Swevers J. On-line time-optimal path tracking for robots. In: IEEE ICRA international conference on robotics and automation; 2009. p. 599–605.
- [30] Hollerbach J, Khalil W, Gautier M. Model identification. In: Siciliano B, Khatib O, editors. Handbook of robotic. Springer; 2008. p. 321–44.
- [31] Tenerz M. Parameter estimation in a permanent magnet synchronous motor. PhD thesis. Sweden: Linköping University; 2011.
- [32] Corke P. A robotics toolbox for MATLAB. *IEEE Robot Autom Mag* 1996;3(1):24–32.
- [33] FunctionBay GmbH. Recurdyn professional. <<http://www.functionbay.de>>; 2012.
- [34] Li Y, Bone G. Are parallel manipulators more energy efficient? In: IEEE international symposium on computational intelligence in robotics and automation, Bannf, CDN; 2001. p. 41–6.
- [35] Giberti H, Cinquemani S, Legnani G. Effects of transmission mechanical characteristics on the choice of a motor-reducer. *Mechatronics* 2010;20(5):604–10.
- [36] ABB, Robotstudio. <<http://www.abb.com/product>>; 2011.
- [37] Meike D, Pellicciari M, Berselli G, Vergnano A, Ribickis L. Increasing the energy efficiency of multi-robot production lines in the automotive industry. In: IEEE International Conference on Automation Science and Engineering Case; 2012. p. 700–5.